Journal Pre-proof

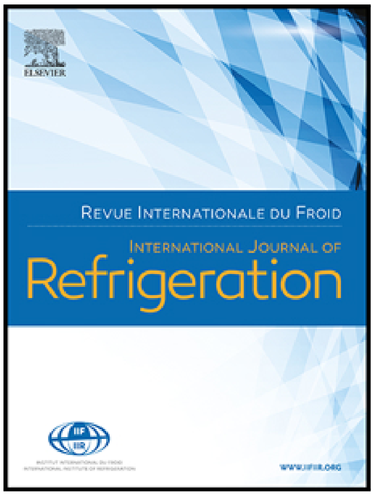

Non-equilibrium approach for the simulation of CO_2 expansion in two-phase ejector driven by subcritical motive pressure

Jakub Bodys, Jacek Smolka, Michal Palacz, Michal Haida, Krzysztof Banasiak

PII: S0140-7007(20)30068-2
DOI: https://doi.org/10.1016/j.ijrefrig.2020.02.015
Reference: JIJR 4674

To appear in: *International Journal of Refrigeration*

Received date: 18 October 2019
Revised date: 6 February 2020
Accepted date: 7 February 2020

Please cite this article as: Jakub Bodys, Jacek Smolka, Michal Palacz, Michal Haida, Krzysztof Banasiak, Non-equilibrium approach for the simulation of CO_2 expansion in two-phase ejector driven by subcritical motive pressure, *International Journal of Refrigeration* (2020), doi: https://doi.org/10.1016/j.ijrefrig.2020.02.015

Highlights

- Non-equilibrium approach for supersonic expansion of carbon-dioxide was presented.
- Phase-change intensity was calibrated on the basis of 150 experimental points.
- High quality of the motive nozzle mass flow rate prediction was obtained.
- Field results were analysed having regard vapour quality and velocity distribution.

This is the accepted version of an article published in International Journal of Refrigeration
https://doi.org/10.1016/j.ijrefrig.2020.02.015

Non-equilibrium approach for the simulation of CO_2 expansion in two-phase ejector driven by subcritical motive pressure

Jakub Bodys[a,*], Jacek Smolka[a], Michal Palacz[a], Michal Haida[a], Krzysztof Banasiak[b]

[a] *Silesian University of Technology, Gliwice, 44-100, Poland*
[b] *SINTEF Energy Research, Trondheim, 7465, Norway*

Abstract

A non-equilibrium approach was proposed for highly accurate modelling of the expansion process during two-phase flow in the convergent-divergent motive nozzle of an R744 ejector. Comprehensive mapping of the coefficients used in the source terms of the additional transport equation of the vapour quality was provided on the basis of four ejector geometries. The calibration range contained motive pressures from 50 bar to 70 bar, where the prediction quality of the homogeneous equilibrium (HEM) and relaxation (HRM) models, was unsatisfactory. The calibrated model was validated on the basis of experimental mass flow rate data collected from 150 operating points. The mapping results were utilised for final model derivation in the form of an approximation function for R744 expansion. The validation process resulted in satisfactory relative error below 10% for the vast majority of the cases. Moreover, 70% of the simulated cases were considered with a mass flow rate discrepancy below 7.5% in the inaccuracy. Finally, the selected cases were compared and discussed with the HEM approach on the basis of field results.

Keywords: transcritical ejector, two-phase expansion, non-equilibrium model, refrigeration system, R744, carbon dioxide

* Corresponding author
Email address: jakub.bodys@polsl.pl Tel:. +48322372341 (Jakub Bodys)

Preprint submitted to International Journal of Refrigeration *February 11, 2020*

This is the accepted version of an article published in International Journal of Refrigeration
https://doi.org/10.1016/j.ijrefrig.2020.02.015

1. Introduction

1.1. Natural refrigerants for refrigeration

The phase-down of synthetic refrigerants from CFC (chlorofluorocarbon) and HFC (hydrofluorocarbon) groups was started by Montreal Protocol United Nations Environment Programme (UNEP) (1987) and pushed forward by a meeting in Kyoto United Nations Framework Convention on Climate Change (UNFCCC) (1997) and EU regulations European Commission (2014). Currently ratified by the European Commission (2018), the Kigali Amendment has been enforced since the first day of 2019, making the phase-in of natural refrigerants an even more global initiative.

Analysis of possible alternative refrigerants with low Global Warming Potential (GWP) concluded that natural refrigerants can overcome HFC and HFO (hydrofluoroolefin) mixtures (Mota-Babiloni et al., 2015),(Purohit et al., 2017). In the case of the main natural representative carbon dioxide (CO_2, R744), one challenge is the application in hot climates due to its thermodynamic properties. Hence, substantial improvement in the CO_2 refrigeration technology was pushed by the academic and industry sectors.

1.2. Ejectors in CO_2 refrigeration

The development of ejector technology has become an increasingly substantial part of the state-of-the-art R744 refrigeration. Elbel and Lawrence, in a comprehensive review of ejector technology in vapour-compression refrigeration systems (Elbel and Lawrence, 2016), confirmed that cutting-edge refrigeration is strongly connected with highly efficient ejectors. Moreover, these authors concluded that there is still substantial potential to improve the ejector systems with regard to the relations between the ejectors and other system components. Another analysis of the current achievements and future perspectives in the ejector technology was presented in the work of Besagni (2019). That study contains a comprehensive review of current and possible ejector implementations. One of the developing areas is related to small units designed for low ambient temperatures and thus low motive pressures between 50-60 bar, such as refrigerated sea water chillers (Bodys et al., 2018).

1.3. Computational approaches for the CO_2 ejector modelling

Advanced tools from the scope of computational fluid dynamics were formulated by Smolka et al. (2013) and Lucas et al. (2014). The authors of these

This is the accepted version of an article published in International Journal of Refrigeration
https://doi.org/10.1016/j.ijrefrig.2020.02.015

studies used the homogeneous equilibrium model (HEM) assumption to simulate two-phase flow inside an ejector. In this approach, mechanical and thermodynamic equilibrium between the phases is assumed to result in instantaneous evaporation processes. The described approach is suitable for high motive pressures above the critical point where meta-stability effects are negligible. In the study of Smolka et al. (2013), the commercial software Ansys Fluent was used, whereas in the study of Lucas et al. (2014) OpenFOAM environment was used. Both approaches allowed for the mass flow rate determination at every port of the ejector. The validation process resulted in motive nozzle mass flow rate (m_{MN}) prediction with accuracy on an average level of 10%. In the case of the suction nozzle stream, Smolka et al. (2013) reported approximately 20% for the suction nozzle mass flow rate prediction. In the study of Lucas et al. (2014), the simulation result was the pressure lift recovery also at the level of 20% of accuracy.

The accuracy of the HEM approach proposed by Smolka et al. (2013) was described extensively in a work by Palacz et al. (2015), where the authors simulated a wide range of operating conditions (OC) and compared the experimental data. The authors focused on the relation between the motive and the suction conditions and the resulting accuracy of the mass flow rate prediction. The results showed that motive nozzle conditions are more crucial and can be described as one of the main parameters that influence the prediction accuracy of the m_{MN}. Moreover, the HEM approach was described as inaccurate up to 10% for high motive pressures above 75 bar. Decreasing motive pressures up to 60 bar resulted in a decrease in the HEM accuracy to the level of 30%. This trend was correlated with the meta-stability effects in the evaporation process, which occur during expansion in the motive nozzle.

Meta-stability effects during two-phase flow have been reported in the numerical modelling literature. Moreover, advanced two-fluid approaches were formulated for the water flow through the convergent-divergent motive nozzle (Yixiang Liao, 2015). In that study of Yixiang Liao (2015), a simulation of inter-phasial interaction based on the heat transfer, mass transfer and momentum transfer was described. In similar, a complex formulation for flashing flow through a convergent-divergent nozzle was proposed by Dang Le et al. (2018), where the thermal non-equilibrium between phases during the evaporation process was simulated. However, in both studies (Yixiang Liao, 2015; Dang Le et al., 2018), the mixing phenomenon and pressure recovery in the diffuser of the ejector were not investigated. This level of complexity for two-streams flow through the R744 ejector ducts based on the two-fluid approach were not pub-

This is the accepted version of an article published in International Journal of Refrigeration
https://doi.org/10.1016/j.ijrefrig.2020.02.015

lished so far. The reasons could be located in the low computational time required for ergonomic design tools as well as insufficient experimental data for the aforementioned supersonic flow of carbon dioxide. Nevertheless, other approaches were developed in order to model the non-equilibrium phase transition and improve the prediction quality of the motive nozzle mass flow rate. In particular, the homogeneous relaxation model (HRM) approach introduced in the work of Bilicki et al. (1990) was utilised by several authors in the R744 simulations. The HRM model equipped in a formulation for the relaxation time allowed for a delayed evaporation process, consequently leading to a higher motive mass flow rate. Some first comparison of the HEM and HRM approaches was delivered by Downar-Zapolski et al. (1996) where the HRM approach was characterised as more accurate with regard to critical mass flow rate prediction, which was underestimated in the HEM simulations. The HRM approach was adjusted for the R744 simulations in the work of Angielczyk et al. (2010) and Colarossi et al. (2012). The accuracy of the motive mass flow rate prediction was still more than 10% for subcritical motive pressures. To extensively compare the HEM and HRM approaches, Palacz et al. (2017a) implemented the HRM formulation proposed by Angielczyk et al. (2010) onto the *ejectorPL* platform described by Palacz et al. (2017b). The HRM results were compared to the experimental data described in the previous work (Palacz et al., 2015) where the HEM approach accuracy was mapped. That comparison proved that the introduction of the relaxation time for a vapour quality field improves the motive mass flow rate prediction by up to 5% for motive pressures higher than 65 bar. The authors concluded that the definition of the time relaxation should be adjusted for specific conditions with regard to model constants proposed by Angielczyk et al. (2010). Further improvement in the mass flow rate prediction accuracy was delivered in the work of Haida et al. (2018c), where some modification of the previously proposed HRM approach was described. The authors adjusted the coefficients in the relaxation time definition, obtaining high accuracy for motive pressure from 59 bar to 80 bar. In this region, the average accuracy was 15%. Nevertheless, accuracy in regions below 59 bar of the motive pressure still needs to be improved to provide proper computing tools for designing the process of subcritical R744 ejectors.

A more advanced formulation of the phase change modelling in the R744 ejector was proposed in the work of Yazdani et al. (2012). A standard set of governing equations for continuity, momentum and energy supported by the additional vapour volume fraction was used. In the study of Yazdani et al. (2012), the approach called mixture was based on cavitation and boiling vapour gener-

This is the accepted version of an article published in International Journal of Refrigeration
https://doi.org/10.1016/j.ijrefrig.2020.02.015

ation, where the first term was proposed by Singhal et al. (2002) and the second was modelled according to the multi-phase flow handbook (Carey, 2007). In the case of both cavitation and boiling source terms, the coefficients need to be arbitrarily assumed. The authors did not describe the procedure of the coefficient assessment. The obtained pressure distribution along the ejector axis was validated against experimental data delivered by Nakagawa et al. (2009) with positive results showing high potential of the approach utilised. On the other hand, the authors did not analyse model accuracy in the subcritical region of the motive pressures where the aforementioned HEM and HRM inaccuracy was relatively high. Finally, the capabilities of the approach proposed by Yazdani et al. (2012) were limited to the prediction of mass entrainment ratio and pressure lift for given motive conditions. In the work of Giacomelli et al. (2018), the HEM approach described in the previous work (Giacomelli et al., 2016) was extended into the mixture approach similar to that used by Yazdani et al. (2012). The HEM approach was based on the enthalpy-based energy equation and real gas properties in compressible flow as previously proposed in the work of Smolka et al. (2013). However, the HEM approach studied by Giacomelli et al. (2016) and by Giacomelli et al. (2018) was not validated in such a wide range of OCs as in the case of Palacz et al. (2015). Moreover, the average accuracy in the mass flow rate prediction was 15%, which was slightly higher than that obtained during validation processes presented in the papers of Smolka et al. (2013) and Palacz et al. (2015). Hence, the mixture approach of Giacomelli et al. (2018) was adjusted to improve the accuracy of the HEM method. Accuracy was improved and equal to a level below 3%, proving the high potential of the mixture approach. Nevertheless, in that investigation, only two sets of supercritical OCs at the motive port were taken into account. Moreover, analysis of the coefficients used in the vapour quality source terms led to inconsistent conclusions. That is, during the sensitivity analysis of the coefficients, its influence was described as negligible. However, in further analysis, the values of the coefficients were multiplied by 6 to match the experimental mass flow rate. Unfortunately, this matter was not studied further. Hence, a more detailed investigation of the applicability of the mixture model in the whole operational envelope of CO_2 ejectors is required.

In this study, the non-equilibrium approach for the R744 ejector was proposed and validated in the subcritical region of the motive pressures, resulting in high accuracy of the predicted motive mass flow rates. The HEM approach was developed, described and extensively validated in previous works (Smolka et al., 2013; Palacz et al., 2015) and was extended by the transport equation

This is the accepted version of an article published in International Journal of Refrigeration
https://doi.org/10.1016/j.ijrefrig.2020.02.015

of the vapour mass fraction. On a basis of the source term in the aforementioned equation, a boiling phenomenon in the phase-change process was modelled. Hence, homogeneous non-equilibrium model with boiling phenomenon (HNB) is presented in this study. To validate the model, comprehensive mapping of the coefficients used in the source terms was provided. Then, to improve practical use of the formulated model, the approximation functions were developed for the R744 expansion process on the basis of the model coefficient maps. Finally, the accuracy of m_{MN} prediction of the developed model was below 10% for the vast majority of examined cases. The results and discussion included description of the field and mass flow rate differences between the HNB and the HEM, noting the region where both models should be used with regard to high accuracy.

2. Investigated envelope of the motive nozzle operation

According to the aforementioned literature, one of the main goals in ejector modelling is to predict the motive and suction nozzle streams to meet the application and properly fit this component into the system cycle. From the fluid mechanics and thermodynamics points of view, the quality of the motive nozzle and suction nozzle mass flow rate prediction is strongly related to the two-phase flow and mixing models applied for the ejector modelling. In particular, the fidelity of the m_{MN} prediction depends mostly on the two-phase flow model applied, while the suction nozzle mass flow rate and entrainment rate prediction are mostly related to turbulence model fidelity. In this study, the authors decided to focus on the motive mass flow rate, while future studies will consider the suction stream analysis. Hence, the investigation is based on the highly accurate modelling of the expansion process during two-phase flow in the convergent-divergent motive nozzle of the R744 ejector. In this matter, one of the key parameters is a proper prediction of the vapour quality distribution along the ejector axis. A procedure for the quality evaluation of the model predicting capabilities for the specific operating range is described in this section.

2.1. Performance factors of the ejector

The ejector operation can be described using the ratio between the mass flow rate at the suction and motive port. This factor is called the mass entrainment ratio (MER):

$$\chi = \frac{m_{SN}}{m_{MN}} \tag{1}$$

This is the accepted version of an article published in International Journal of Refrigeration
https://doi.org/10.1016/j.ijrefrig.2020.02.015

where χ is the mass entrainment ratio and m is the mass flow rate of the motive nozzle (MN) and the suction nozzle (SN). The most common definition of ejector efficiency was proposed by Elbel and Hrnjak (2008). That formulation is a ratio of the amount of the recovered ejector expansion work rate (subscript rec) to the maximum possible expansion work rate recovery potential (subscript rec, max):

$$\eta_{ej} = \frac{W_{rec}}{W_{rec,max}} = \chi \cdot \frac{h(p_{OUT}, s_{SN}) - h(p_{SN}, s_{SN})}{h(p_{MN}, s_{MN}) - h(p_{OUT}, s_{MN})} \tag{2}$$

where η_{ej} is the ejector efficiency, W is the expansion work rate, s is the specific entropy and the subscript OUT denotes the ejector outlet.

2.2. Accuracy definition

With regard to the numerical approach utilised in this study (detailed description given in Section 4), one of the main model deliverable data set is that of the motive stream and the suction stream. Hence, a quantification of the model accuracy is mostly based on the relative error between the experimental data and the model predictions:

$$\delta m = \frac{m_{CFD} - m_{EXP}}{m_{EXP}} \cdot 100\% \tag{3}$$

where δm is the relative error of the selected flow parameter obtained by the CFD model (subscript CFD) compared to the experimental (subscript EXP) data.

2.3. Model accuracy regions in the R744 ejector envelope

Considering the literature review and the current state-of-the-art R744 ejector numerical models, the applied model accuracy is strongly related to the motive nozzle absolute pressure. Decreasing motive pressure and temperature have a crucial impact on the accuracy deterioration when the mass flow rate of the motive port is taken into consideration. An underestimation of the m_{MN} is observed for both the HEM and HRM approaches (Palacz et al., 2015; Haida et al., 2018c). Hence, with regard to motive pressure, the highest accuracy of the HEM approach is obtained above the critical pressure of carbon dioxide, while HRM provides high-quality predictions for the subcritical parameters at the motive nozzle inlet. To the authors' best knowledge, the most extensive validation of the HEM approach was delivered in the works of Palacz et al. (2015), including the region from 47 bar to 95 bar and from 6 °C to 36 °C at the motive nozzle inlet. The aforementioned region corresponds to the area marked

This is the accepted version of an article published in International Journal of Refrigeration
https://doi.org/10.1016/j.ijrefrig.2020.02.015

by green and red frames in Fig. 1. According to those studies, the average HEM accuracy in the high-pressure region (green frame) in Fig. 1 is on the level of 6.4%. Simultaneously, the HEM approach becomes substantially deteriorated, with an average accuracy of 24.1% for the motive pressures below the critical point marked by the red frame. Moreover, the maximum reported inaccuracy was 52.0%. In this region of lower motive pressure, the HRM approach improved prediction accuracy to an average level of 20.2% and a maximum of 29.0% (Palacz et al., 2017a; Haida et al., 2018a). Nevertheless, as reported in the work of Haida et al. (2018a), the largest underestimation of the m_{MN} was located below 59 bar of the motive pressure, while in the operating range between 59 bar and 70 bar, the average accuracy was on the level of 6.5%. Nevertheless, due to the relatively high maximum inaccuracies, the whole region below 70 bar was taken into account in a calibration procedure presented in Section 5.2 and finally considered for applicability of the approach developed in this study.

This is the accepted version of an article published in International Journal of Refrigeration
https://doi.org/10.1016/j.ijrefrig.2020.02.015

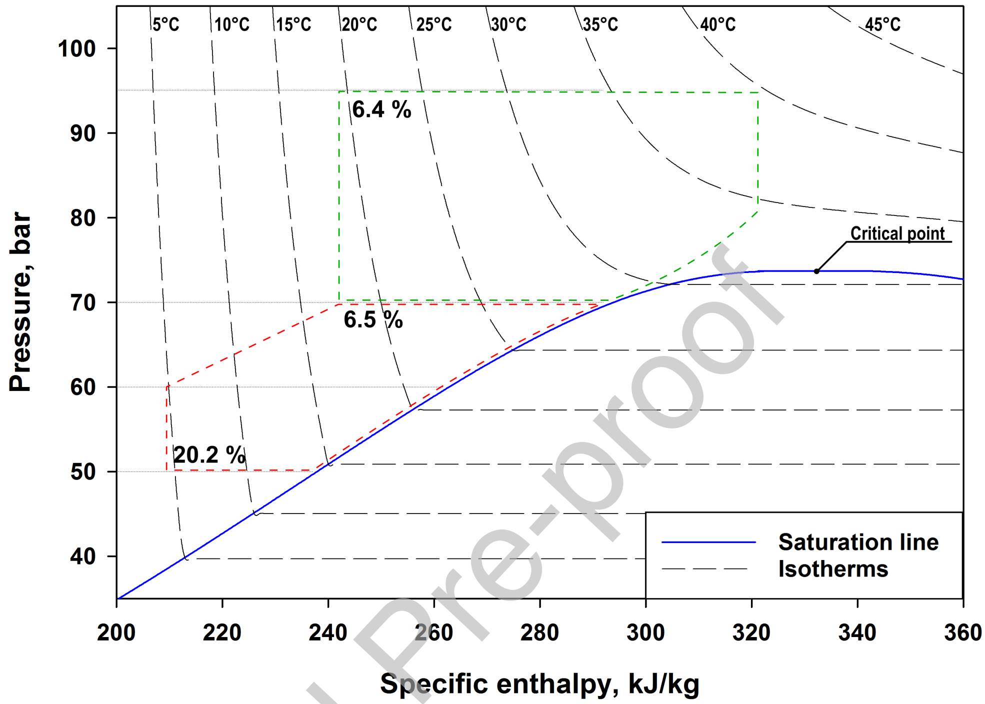

Figure 1: Absolute pressure-specific enthalpy diagram of carbon dioxide with marked regions of the higher (green) and lower (red frame) motive pressure and the average accuracy of the HEM (in green frame) and HRM (in red frame) approaches.

3. Tested ejectors

3.1. Geometry

The ejector domains utilised in this study were investigated extensively in previous experimental works on the multi-ejector module (Banasiak et al., 2015; Haida et al., 2016) and numerical studies focused on validation of the HEM and HRM simulations (Smolka et al., 2013; Palacz et al., 2015, 2017a; Haida et al., 2018a). The ejector motive nozzle is defined according to the geometry presented in Fig. 2. The crucial dimensions of the two motive nozzles utilised in this study were listed in Table 1. The remaining dimensions were established on the basis of aforementioned studies where specific relations between the utilised dimensions are investigated using more detailed approach. Namely, the ejectors were designed for various capacities of the expanding fluid in binary manner. Therefore, as shown in Table 1, the motive nozzle throat cross-section area for motive nozzle B is two times larger than that for motive nozzle A. Moreover, each pair contains the ejector for the low and the high pressure lift applying the same approach for the capacity that is two times higher. Hence, four ejector configurations were investigated to establish the reliable calibration procedure of the model developed in this study.

The numerical domain was obtained on the basis of the commercial software Ansys ICEM CFD. With regard to the axis symmetry of the ejector geometry, the computational domain was generated for 2-D computations. A fully hexahedral numerical mesh was generated according to the high requirements of the transonic flow simulation. The domain was extended before the motive nozzle inlet and after the diffuser outlet to ensure numerical stability of the solution process. The number and distribution of the cells were finally determined on the basis of the analysis in Section 5.1, where the mesh sensitivity study was discussed.

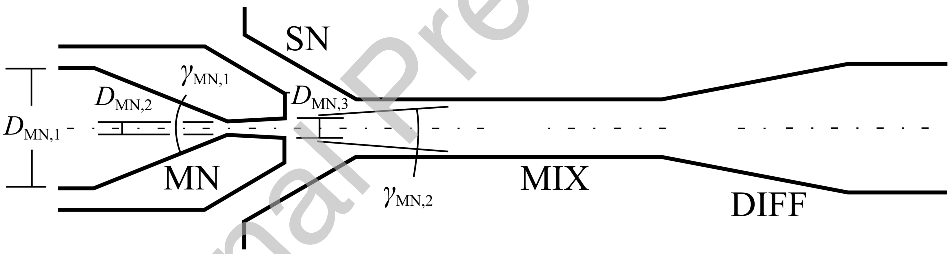

Figure 2: General scheme for a single-ejector geometry: MN motive nozzle section, SN suction nozzle section, MIX mixing section, and DIFF diffuser section.

Table 1: Geometrical parameters of the tested ejector motive nozzles

Parameter name (symbol)	Unit	Value	
		Motive nozzle A	Motive nozzle B
Motive nozzle inlet diameter (D_{MN1})	mm	3.80	3.80
Motive nozzle throat diameter (D_{MN2})	mm	1.41	2.00
Motive nozzle outlet diameter (D_{MN3})	mm	1.58	2.24
Motive nozzle converging angle (γ_{MN1})	°	30.00	30.00
Motive nozzle diverging angle (γ_{MN2})	°	2.00	2.00

This is the accepted version of an article published in International Journal of Refrigeration
https://doi.org/10.1016/j.ijrefrig.2020.02.015

3.2. Operating regimes

The considered ejectors were tested in a laboratory test rig at the SINTEF Energy Research (Trondheim, Norway), which resulted in experimental data that included the mass flow rates at the ejector ports. The whole set of OCs used in this study was reported by Haida et al. (2016). In that work, the experimental procedure and accuracy of the measurements were described. In particular, the measurement accuracy was in range from 0.05 K to 0.3 K for the temperature, ±0.3% of reading for the pressure and ±0.2% of reading for the mass flow rate. The presented ejectors were analysed for the motive nozzle operating regimes marked by the red frame in Fig. 1. The complete set of OC utilised in the model calibration and validation procedures is presented in Table 3 (Appendix A) for motive nozzle A and in Table 5 (Appendix B) for motive nozzle B. Hence, the motive inlet pressure conditions were in the range from 45 bar to 70 bar, and the temperature was between 7 °C and 28 °C. These conditions correspond to the refrigeration unit operation in medium- and high-temperature climates such as the Mediterranean. A subcooling level varied from 0 K up to approximately 15 K. Moreover, in the group of the low pressure lift, the motive nozzle B was simulated with three sets of the motive nozzle conditions very close to the saturation line. The suction port conditions could be assigned for chilling purposes at -1 °C and air conditioning at 10 °C. Consequently, the aforementioned set could be referred, e.g., to supermarket Heating Ventilation and Air Conditioning (HVAC) applications.

To better illustrate the distribution of the operating points, the data contained in Table 3 (Appendix A) and Table 5 (Appendix B) are presented in graphs in Figs. 3 and 4. The motive inlet conditions are marked in Fig. 3a and 3b for motive nozzle geometries A and B, respectively. Moreover, points were grouped into groups of a low (below 4 bar) and high (more than 4 bar) pressure lift defined as a pressure difference between the outlet and the suction port. Similarly, the suction and outlet pressure conditions are illustrated in Fig. 4a and 4b where pressure lift was correlated with the suction nozzle port pressure for given OC. The types of mixing chambers are marked by red dots and green triangles for the high- and low-pressure lift conditions, respectively.

This is the accepted version of an article published in International Journal of Refrigeration
https://doi.org/10.1016/j.ijrefrig.2020.02.015

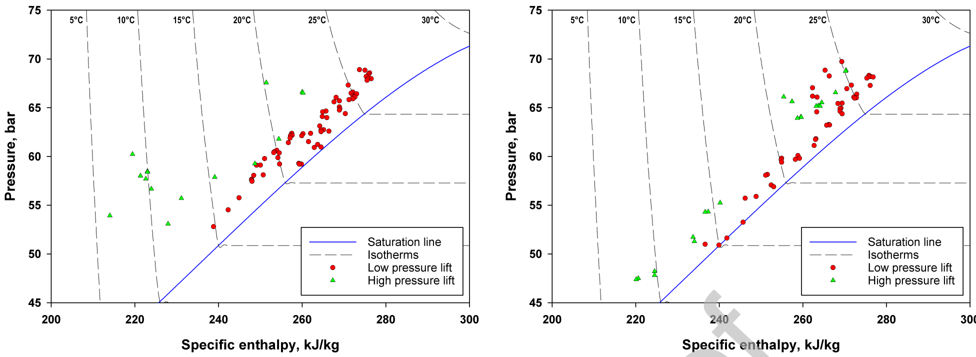

(a) Motive nozzle A (b) Motive nozzle B

Figure 3: Absolute pressure-specific enthalpy diagram of carbon dioxide with marked inlet conditions for (a) motive nozzle A and (b) motive nozzle B.

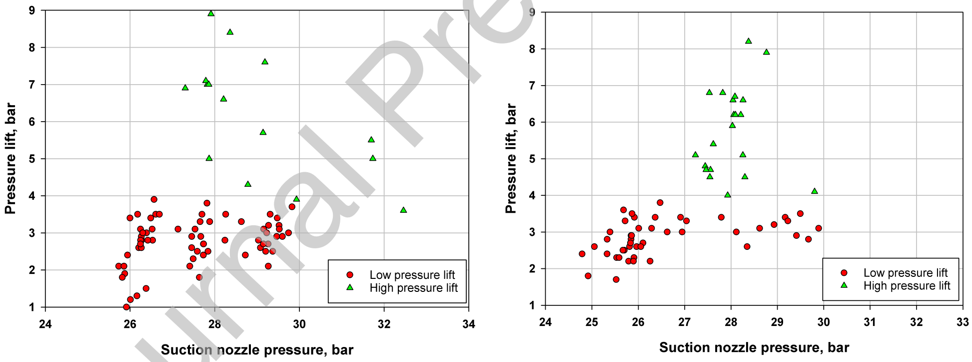

(a) Motive nozzle A (b) Motive nozzle B

Figure 4: OC of the suction nozzle port and the outlet presented on the basis of the pressure lift as a function of the suction nozzle pressure for (a) motive nozzle A and (b) motive nozzle B.

4. Computational procedure

The HNB considered in this study is presented in this Section. This approach was developed on the basis of the mathematical model for two-phase transcritical flow inside the ejector ducts proposed by Smolka et al. (2013). Hence, the HEM approach was extended by an additional transport equation of the

This is the accepted version of an article published in International Journal of Refrigeration
https://doi.org/10.1016/j.ijrefrig.2020.02.015

vapour mass fraction with properly adjusted source terms for a phase change regulation based on the boiling phenomenon. Moreover, formulation of the R744 properties was reconsidered with regard to the full set of governing equations.

4.1. Governing equations of the mathematical model

The two-phase flow inside the ejector was formulated on the basis of the governing equations and assumption of the steady-state simulation (Chung, 2010; Anderson, 1995). The conservation equation of the mass is defined as follows:

$$\nabla \cdot \left(\bar{\rho}\tilde{\mathbf{u}}\right) = 0 \tag{4}$$

where the Reynolds and Favre-averaged quantities are indicated by ($\bar{\ }$) and ($\tilde{\ }$), respectively. Moreover, ρ is the fluid density, and $\mathbf{u}$ is the fluid velocity vector. The momentum balance is defined by the following equation:

$$\nabla \cdot \left(\bar{\rho}\tilde{\mathbf{u}}\tilde{\mathbf{u}}\right) = -\nabla \bar{p} + \nabla \cdot \tilde{\tau} \tag{5}$$

where p is the pressure of fluid and τ is the stress tensor.

According to Smolka et al. (2013), the temperature-based form of the energy equation can be replaced by the enthalpy-based form. Hence, the energy balance of the R744 two-phase flow can be defined as follows:

$$\nabla \cdot \left(\bar{\rho}\tilde{\mathbf{u}}\tilde{E}\right) = \nabla \cdot \left[\left(\frac{\lambda}{\frac{\partial h}{\partial T}}\right)_p \nabla \tilde{h} - \left(\frac{\lambda}{\frac{\partial h}{\partial T}}\right)_p \left(\frac{\partial h}{\partial p}\right)_T \nabla \bar{p} + \tilde{\tau} \cdot \tilde{\mathbf{u}} \right] \tag{6}$$

where T is the mixture temperature, λ is the fluid thermal conductivity and E is the total specific enthalpy defined as a sum of the specific mixture enthalpy and the kinetic energy:

$$\tilde{E} = \tilde{h} + \frac{\tilde{u}^2}{2} \tag{7}$$

where h is the mixture specific enthalpy. Turbulence modelling was provided on the basis of the $k-\epsilon$ *realizable* turbulence model (Shih et al., 1995), as proposed by the base model developed by Smolka et al. (2013). Hence, two additional turbulence equations in the following forms were utilised:

$$\nabla \cdot \left(\bar{\rho}\tilde{\mathbf{u}}k\right) = \nabla \cdot \left[\left(\mu + \frac{\mu_T}{\sigma_k} \nabla k\right) \right] + G_k + G_b - \bar{\rho}\epsilon - Y_M \tag{8}$$

This is the accepted version of an article published in International Journal of Refrigeration
https://doi.org/10.1016/j.ijrefrig.2020.02.015

$$\nabla \cdot \left(\bar{\rho}\tilde{\mathbf{u}}\epsilon\right) = \nabla \cdot \left[\left(\mu + \frac{\mu_T}{\sigma_\epsilon}\nabla\epsilon\right)\right] + C_{1\epsilon}\frac{\epsilon}{k}\left(G_k + C_{3\epsilon}G_b\right) - C_{2\epsilon}\bar{\rho}\frac{\epsilon^2}{k} \tag{9}$$

where k is the turbulent kinetic energy, ϵ is the turbulent dissipation rate, μ and μ_T are the molecular and turbulent dynamic viscosity, σ_k and σ_ϵ are the turbulent Prandtl numbers for k and ϵ respectively, G_k and G_b denote the generation of the turbulence kinetic energy due to mean velocity gradients and buoyancy, respectively, and Y_M represents the contribution of the fluctuating dilatation in compressible turbulence to the overall dissipation rate. The constant C depends on the $k-\epsilon$ model variant.

The vapour quality field in the numerical simulation is tracked by the scalar transport equation including convective and source term. The additional conservation equation of the vapour mass fraction is given as (Singhal et al., 2002):

$$\nabla \cdot \left(\tilde{\rho}\tilde{X}\right) = R \tag{10}$$

where R is the vapour generation rate in and X is the vapour quality, which indicates the vapour mass in the mixture total. This approach is utilised due to requirements of the finite volume method which is used by the flow-dedicated solver. The equation is introduced to the Ansys Fluent solver using functionality of the User-Defined Scalar (Ansys, 2019). The prediction of the mass transfer is located in the source term R on the right-hand of the equation.

4.2. Source term in vapour mass fraction equation

In the state-of-the-art ejector cycles mentioned in Section 1, the saturation line is crossed during the expansion process in the motive nozzle. Hence, the phenomenon of liquid evaporation must be taken into consideration. The aforementioned literature review contains only a few studies in which the transition into the two-phase regime is treated as a non-equilibrium process (Yazdani et al., 2012; Giacomelli et al., 2018). In this study, the evaporation and condensation rate are modelled on the basis of the kinetic theory of phase change (Carey, 2007). According to the kinetic theory (Carey, 2007), the boiling phase change process can be described as the flux of given molecules between the inter-facial surface:

$$j_{nw\pm} = \Gamma(\pm a)\left[\frac{M}{2\pi G_c T}\right]^{1/2} \cdot \frac{p}{f} \tag{11}$$

where $j_{nw\pm}$ is the flux of the molecules, Γ is the formulation correction factor and corresponds to the bulk motion effect, M is the molecular mass of

This is the accepted version of an article published in International Journal of Refrigeration
https://doi.org/10.1016/j.ijrefrig.2020.02.015

the working fluid, G_c is the universal gas constant and f is the mass flux of molecules described by molecular mass M. This equation can be converted to the form that represents mass flux. Finally, on the basis of Carey (2007), the following relation for vapour mass generation rate was implemented to the vapour mass fraction equation:

$$R = \pm \left[\frac{\widehat{\sigma}}{2 - \widehat{\sigma}} \right] \left(\frac{M}{2\pi G_c T_{sat}} \right)^{1/2} \left[p - p_{sat} \right] \tag{12}$$

where T_{sat} is the local saturation temperature and p_{sat} is the saturation pressure obtained for isentropic expansion from the motive nozzle inlet conditions. That approach was utilised in the study presented by Haida et al. (2018c). The coefficient $\widehat{\sigma}$ is the accommodation coefficient that represents the number of molecules passing during the phase change process. The aforementioned $\widehat{\sigma}$ needs to be adjusted according to the experimental data. Moreover, the value of that coefficient varies with the motive nozzle OC and the selected working fluid. It is worth mentioning that the mapping of $\widehat{\sigma}$ for various ejector designs and working fluids may be beneficial from an ejector modelling point of view. This procedure was performed in this study (Section 5.2) for carbon dioxide and OC, where a non-equilibrium phase change is expected.

4.3. Computations of one-phase and mixture properties

The properties of the real fluid are obtained from the REFPROP ver. 9 libraries on the basis of the approach presented by Lemmon et al. (2010). In the one-phase regions, local state variables are a function of pressure and enthalpy (Smolka et al., 2013):

$$\left\{ \rho, \mu, \lambda, c_p \right\} = f\left(p, h\right) \tag{13}$$

where μ is the dynamic viscosity and c_p is the specific heat. In the two-phase region, where thermal and mechanical equilibrium exists between the phases, saturation variables are a function of pressure and enthalpy (Stadtke, 2006):

$$\left\{ \rho_g, \rho_l, \mu_g, \mu_l, \lambda_g, \lambda_l, c_{p,g}, c_{p,l} \right\} = f\left(p\right) \tag{14}$$

where subscripts g and l denote saturated gas and saturated liquid conditions, respectively. The mixture quantities are obtained on the basis of an additional third independent parameter, i.e., the vapour mass fraction (Stadtke, 2006):

$$\left\{ \rho, \mu, \lambda, c_p \right\} = f\left(p, X\right) \tag{15}$$

This is the accepted version of an article published in International Journal of Refrigeration
https://doi.org/10.1016/j.ijrefrig.2020.02.015

The final formulations for mixture state properties in the governing equations are defined as follows Stadtke (2006):

$$\rho = \frac{1}{X/\rho_g + (1-X)/\rho_l} \tag{16}$$

$$\mu = \frac{1}{X/\mu_g + (1-X)/\mu_l} \tag{17}$$

$$\lambda = \frac{1}{X/\lambda_g + (1-X)/\lambda_l} \tag{18}$$

$$c_p = \frac{1}{X/c_{p,g} + (1-X)/c_{p,l}} \tag{19}$$

The described formulations were used for the R744 flow calculation in single- and two-phase flow conditions for subcritical, transcritical and near-critical point conditions (Smolka et al., 2013; Palacz et al., 2015).

4.4. Boundary conditions for numerical simulation

The pressure-based boundary conditions were used for the motive nozzle and suction nozzle inlets and the outlet of the two-phase ejector. With regard to the enthalpy-based energy equation, the specific enthalpy needed to be specified at each port as well. The OC presented in Table 3 (Appendix A) and in Table 5 (Appendix B) were used to generate pressure-enthalpy sets for the boundary conditions at each port. Next, the pressure-enthalpy conditions were used to define the value for the quality transport equation at the motive and suction nozzle inlet. Hence, the value at the motive port was 0 due to the subcooled liquid region and the value at the suction port was 1 due to the superheated vapour region. According to the previous studies, the turbulence intensity was assumed to be 10% for both motive and suction inlet. Finally, the hydraulic diameter was calculated separately for each inlet according to the geometrical dimension of each nozzle. The walls of the ejector were simulated as an adiabatic surface. The roughness of the wall surface was set to 2 μm as declared by the ejector manufacturer. According to the turbulence model, the standard wall treatment was used to model the boundary layer.

This is the accepted version of an article published in International Journal of Refrigeration
https://doi.org/10.1016/j.ijrefrig.2020.02.015

4.5. *Implementation into ejectorPL platform*

The model was implemented in the *ejectorPL* platform developed during the HEM accuracy mapping presented in Palacz et al. (2015) and utilised for the ejector shape optimisation study presented in Palacz et al. (2017b). The computational platform was updated by the HRM model (Palacz et al., 2017a), the heat transfer module of thermal analysis within the ejector wall (Haida et al., 2018a) and the snapshot generator for reduced order models (Haida et al., 2018b). The platform provides repeatable simulations of the ejectors for various working fluids through the utilisation of commercial software Ansys ICEM CFD 18.2 and Ansys Fluent 18.2. The structure of the platform was slightly modified according to the model developed in this study. The current structure of this tool is presented in Fig. 5, where the implemented modification is marked in green. Hence, the platform provides a full path from geometry preparation through numerical discretisation, solving process and post-processing of the computational results. The complete path from the geometry preparation to the final results costs approximately 45 minutes when taking into account the mesh selected from the mesh independence study (Section 5.1). Differences in computational time between solutions obtained for various boundary conditions are negligible. However, the coarser mesh generated directly from the *ejectorPL* platform takes approximately 20 minutes less of computational time than the case with the finer mesh. Moreover, due to the improved solver algorithms, the time of coarser mesh simulation with the HNB approach is comparable to the time of simulations with the HEM approach. The vast majority of the computing cost is the solving process, which is realised on the 10 computing cores contained in a cluster located at the Institute of Thermal Technology of the Silesian University of Technology, Gliwice, Poland. At the end of the solving process, the levels of the residuals were below a value of 10^{-5} for all the governing equations. Additionally, a mass imbalance was monitored until its level was reduced to below 0.01% of the suction nozzle mass flow rate.

This is the accepted version of an article published in International Journal of Refrigeration
https://doi.org/10.1016/j.ijrefrig.2020.02.015

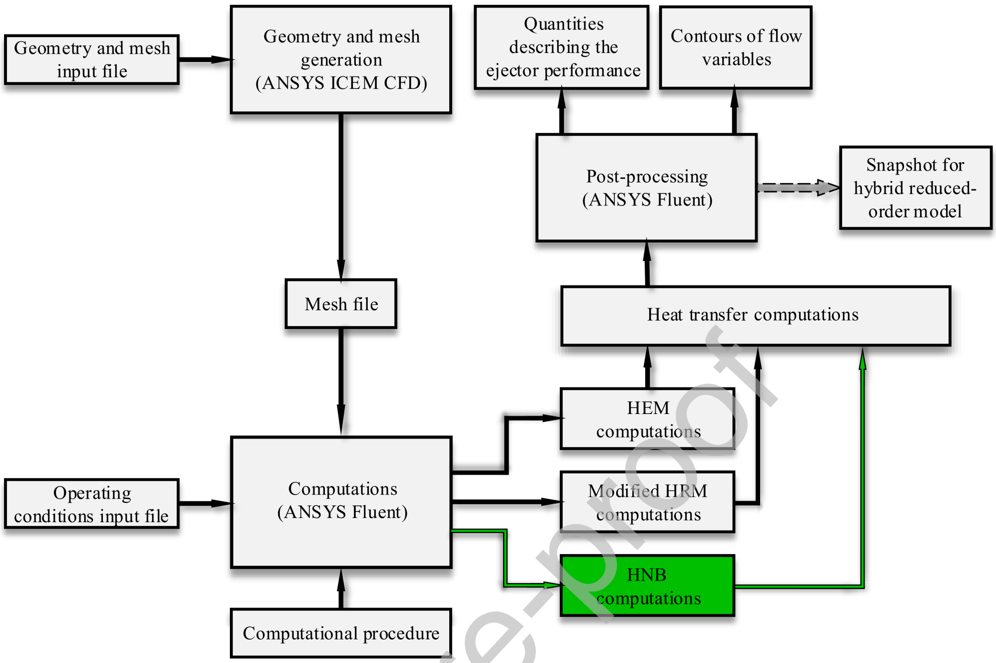

Figure 5: Flowchart of the *ejectorPL* platform with implemented path (green) for the HNB computations, modified and adapted from Palacz et al. (2015) Haida et al. (2018a)

5. Model calibration

5.1. Mesh independence study

As mentioned in Section 4.5, for both the HEM and HNB, the computational procedure was carried out by the developed platform, including the automatic generation of the fully structural numerical mesh for which the independence study was provided in the previous studies. These studies considered mesh independence study in transcritical states of the motive nozzle inlet. The obtained structural mesh was characterised by minimal orthogonal quality factor (defined according to the utilised software documentation (Ansys, 2019)) at the level of 0.85 and maximum aspect ratio of 2.5 in the flow direction. The distribution and number of elements were on a satisfactory level regarding ergonomic of the simulations characterised by the computational time. Nevertheless, to ensure the reliability of the new model analysis, additional mesh refinement was examined. Hence, the baseline numerical mesh generated by the *ejectorPL* code was refined and simulated to compare the difference between

This is the accepted version of an article published in International Journal of Refrigeration
https://doi.org/10.1016/j.ijrefrig.2020.02.015

the aforementioned standard distribution. The results of the mesh independence study are listed in Table 2. The analysis contained two sets of boundary conditions for the smaller motive nozzle geometries, #4 and #77 (see Table 3 in Appendix A). These points were chosen as representatives of high and low motive nozzle pressures, respectively. Both the HEM and HNB approaches were analysed. $\widehat{\sigma}$ for the high quality of the motive mass flow rate prediction (δm below 0.5%) has already been chosen on the basis of further analysis given in Section 5.2.

The baseline mesh of the *ejectorPL* was built on the basis of over 45,000 elements. The final refined mesh contained over 80,000 elements. In each case, the relative difference δm in the mass flow rate value was lower than 0.5%. Moreover, a maximum difference between local absolute pressure and specific enthalpy values along the motive nozzle profile was below 1%. The described differences were evaluated as low enough, taking the previous validation of the developed model into account (Palacz et al., 2015). Nevertheless, with regard to the acceptable computational time of the refined mesh at the level of 45 minutes and the high quality of the fields, the refined mesh was chosen for further investigation.

Table 2: Mass flow rates at the motive nozzle inlet for the analysed mesh variants

			ejectorPL	
			base	refined
HEM	#4	m, kg·s^{-1}	0.0560	0.0558
		δm,%	-	-0.467
	#77	m, kg·s^{-1}	0.0512	0.0510
		δm,%	-	-0.438
HNB	#4	m, kg·s^{-1}	0.0570	0.0567
		δm,%	-	-0.454
	#77	m, kg·s^{-1}	0.0777	0.0774
		δm,%	-	-0.489

5.2. Calibration of the model on the basis of the $\widehat{\sigma}$ mapping

The model calibration was conducted with regard to the experimentally determined mass flow rates for the given OC. The values of the coefficients determine the intensity of the phase change. An increment in the coefficients results in more intensive evaporation and lower pressure in the motive nozzle throat. Consequently, the model prediction of the motive mass flow rate is adjusted.

This is the accepted version of an article published in International Journal of Refrigeration
https://doi.org/10.1016/j.ijrefrig.2020.02.015

In the calibration procedure, all 150 OCs for the two motive nozzles were taken into account. The calibration procedure was performed with regard to the accuracy of the mass flow rate prediction δm below 0.5%. In that procedure, the *ejectorPL* platform was utilised for serial computations with an in-house developed script to search for the $\widehat{\sigma}$. The obtained $\widehat{\sigma}$s are presented in Table 4 (Appendix A2) and Table 6 (Appendix B2) and were tuned based on the experimental data presented in Table 3 (Appendix A) and in Table 5 (Appendix B). The graphical representation of Table 4 and Table 6 is available in Fig. 6, where the values of the coefficients are marked on the pressure-enthalpy diagram. In this figure, the chosen values of the coefficients are located in the corresponding points as presented in Fig. 6.

The values of the coefficients are between 0.28 and 1.54. Moreover, there is a correlation between the absolute pressure, the specific enthalpy and the coefficient values. The coefficient values decrease with decreasing pressure and enthalpy. From a physical point of view, the phase change is less instantaneous in the lower-pressure region. Simultaneously, higher-pressure regions result in more dynamic or even instantaneous evaporation processes. This behaviour is expected with regard to HEM assumptions and its high accuracy only in the region of the high motive pressures (see Fig. 1).

This is the accepted version of an article published in International Journal of Refrigeration
https://doi.org/10.1016/j.ijrefrig.2020.02.015

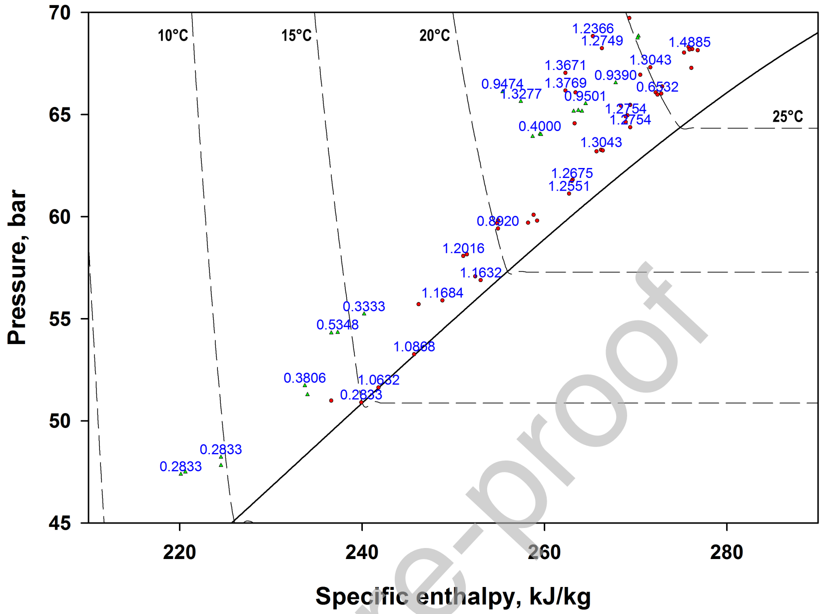

(a) Motive nozzle *A*

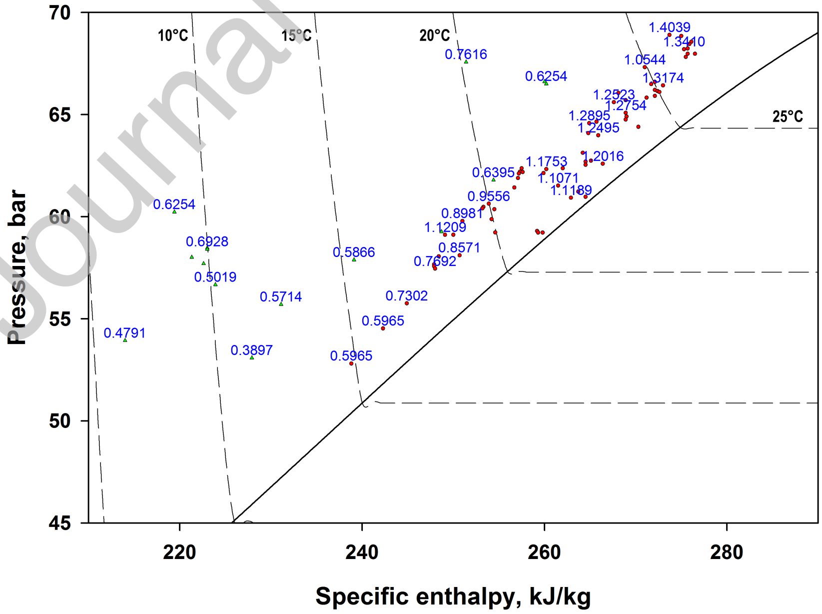

(b) Motive nozzle *B*

Figure 6: $\widehat{\sigma}$ on the pressure-enthalpy diagram of carbon dioxide for (a) motive nozzle A and (b) motive nozzle B.

This is the accepted version of an article published in International Journal of Refrigeration
https://doi.org/10.1016/j.ijrefrig.2020.02.015

5.3. Approximation function of the $\widehat{\sigma}$

According to the model applicability, the necessity of manual coefficient adjustment should be evaluated as a form of model limitation. Hence, the calibration results were utilised for the development of the function $\widehat{\sigma}_{map}$. The paraboloid function was prepared for computations of the $\widehat{\sigma}$ values. Statistical tools available in the commercial software SigmaPlot v. 14.0 (Systat Software Inc.) were utilised for function determination. The resulting formulation is presented in Eq. (20). The function utilises the absolute pressure and specific enthalpy at the motive nozzle inlet. The function reflects the general trend with regard to a negligible number of non-matching points. Global evaluation of goodness of fit was prepared in the form of coefficient of determination, for which a value of 0.9127 was obtained.

$$\widehat{\sigma}_{map} = 3.16978 - 0.119943 \cdot P_{MN} - 0.0650588 \cdot h_{MN} - 0.000790122 \cdot P_{MN}^2 + 0.000153503 \cdot h_{MN}^2 \tag{20}$$

As mentioned, some of the obtained $\widehat{\sigma}$ values did not fit into the general trend. However, the number of calibration points was large enough to minimise the influence of these points. A graphical illustration of the obtained $\widehat{\sigma}$ distribution (red dots) is presented in Fig. 7. Moreover, the developed function $\widehat{\sigma}_{map}$ is presented in the form of a surface (blue mesh). In Fig. 7, there are two views where local discrepancies are visible from the point of view of the specific enthalpy and absolute pressure.

https://doi.org/10.1016/j.ijrefrig.2020.02.015

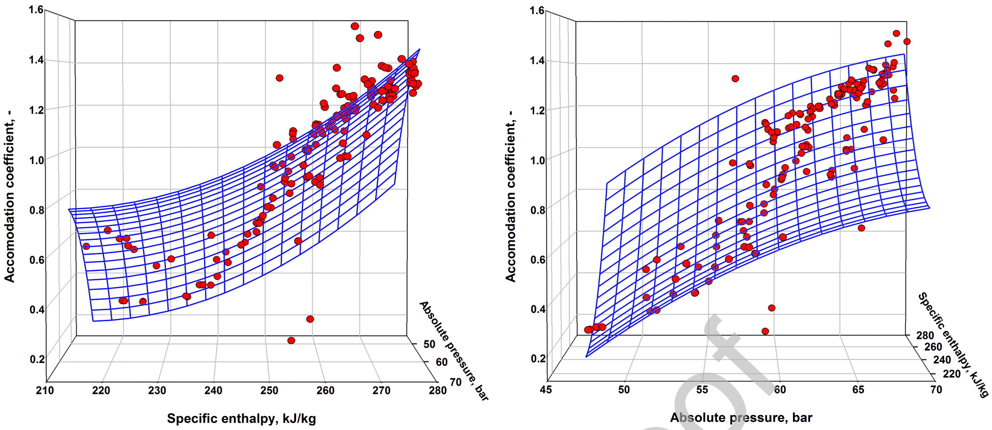

(a) Specific enthalpy view (b) Absolute pressure view

Figure 7: The adjusted $\widehat{\sigma}$ (red dots) on a pressure-specific enthalpy graph where the approximation function is presented as a blue surface for (a) the specific enthalpy view and (b) absolute pressure view.

5.4. *HNB with the approximation function*

Another computational campaign with the same set of boundary conditions was conducted using the approximation function $\widehat{\sigma}_{map}$ for the reproduction of the $\widehat{\sigma}$ values. The results of this analysis are illustrated in Fig. 8a for motive nozzle A and in Fig. 9a for motive nozzle B. Moreover, the resulting dynamics of the evaporation process and the accuracy of the m_{MN} prediction were correlated with the corresponding $\widehat{\sigma}$. Additionally, the distribution of the model accuracy is presented in Fig. 8b and in Fig. 9b for the smaller (A) and larger (B) motive nozzles, respectively.

First, the developed function $\widehat{\sigma}_{map}$ reproduces $\widehat{\sigma}$ however the $\widehat{\sigma}$ values from the function are not identical with the values from mapping procedure. This discrepancy is presented by the grey bars in Fig. 8a and Fig. 9a. The differences between the 'in-point' calibrated coefficient and the approximated coefficient are significant and in some cases exceed ±30%. Nevertheless, in most cases, the function computes the coefficient value with a difference lower than ±15%.

The expected correlation between the accommodations coefficient values and the obtained mass flow rate is clearly visible. That is, when the function $\widehat{\sigma}_{map}$ computes an excessively high coefficient value, the resulting mass flow rate is too low, and vice versa, an excessively high mass flow rate is obtained when the coefficient value is too low. Nevertheless, the difference between the

This is the accepted version of an article published in International Journal of Refrigeration
https://doi.org/10.1016/j.ijrefrig.2020.02.015

calibrated and computed $\widehat{\sigma}$ does not result in the same difference in the mass flow rate accuracy. Moreover, the relation is not linear and is not proportional between the investigated cases. That is, the same difference between the calibrated and computed $\widehat{\sigma}$ can result in variation in the accuracies of the mass flow rate prediction. For example, simulation of boundary conditions #53-54 of smaller motive nozzle A resulted in different mass flow rate accuracies despite the reproduction of the $\widehat{\sigma}$ obtained with almost the same accuracy. This behaviour might imply that the evaporation process is not completely constrained by the coefficient value and that the influence of the flow parameters is still visible.

As shown in Fig. 8 and Fig. 9 by the red dot bars and red dots, high accuracy within ±7.5% was obtained for motive nozzle A with regard to the motive nozzle type and resulting accuracy levels. The results of motive nozzle B are more dispersed and could be characterised as more non-uniform than those obtained from the smaller motive nozzle A. Finally, in the vast majority of the cases reaching 90%, the accuracy of the mass flow rate prediction was below ±12.5%. The group of the smaller motive nozzle contains three cases with an inaccuracy on the level of ±13.5%.

Motive nozzle B resulted in two cases that exceeded ±12.5% with 50.5% (OC #52) and 15.1% (OC #3). The boundary condition related to the highest error is characterised by motive conditions very similar to the saturation line of the liquid where the measured sub-cooling was lower than 1 K. This situation might disturb the mass flow rate measurement due to the very sensitive characteristic of the Coriolis mass flow-meter for which homogeneous flow without gas bubbles should be ensured. Finally, with regard to the total number of simulated cases, only one case was characterised by the m_{MN} prediction significantly exceeding ±15.0%.

This is the accepted version of an article published in International Journal of Refrigeration
https://doi.org/10.1016/j.ijrefrig.2020.02.015

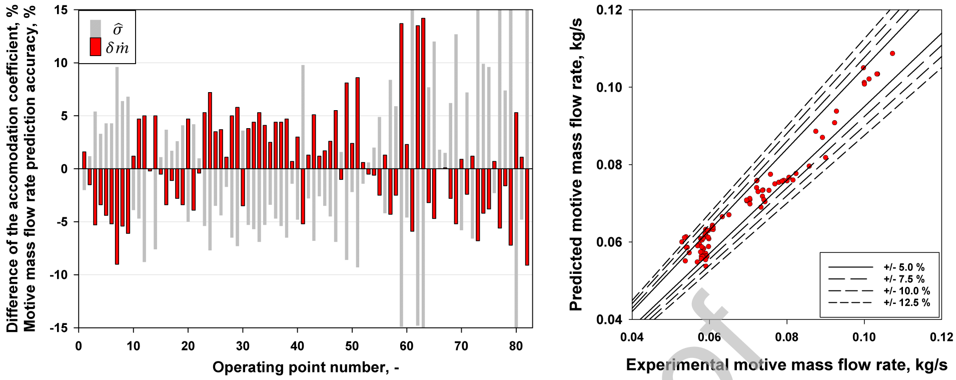

(a) Accuracy of each considered operating point (b) Accuracy distribution

Figure 8: Accuracy of (a) $\hat{\sigma}$ reproduction via the $\hat{\sigma}_{map}$ function (grey bars) and mass flow rate prediction (red bars) and (b) resulting accuracy dispersion of the motive mass flow rate prediction for motive nozzle A.

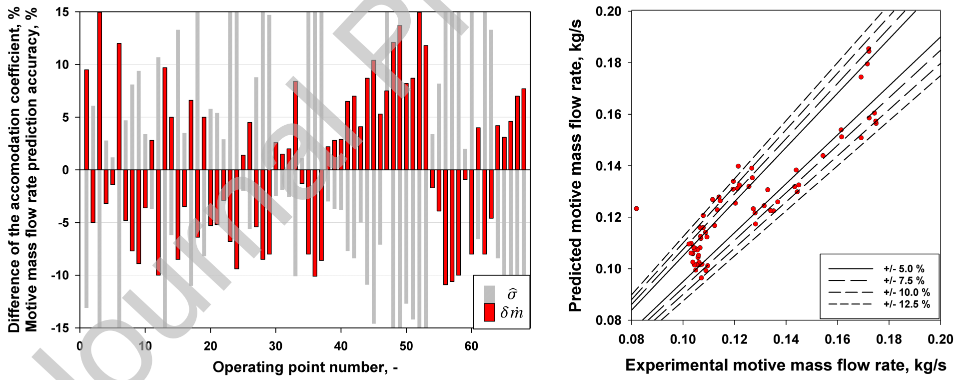

(a) Accuracy of each boundary condition (b) Accuracy distribution

Figure 9: Accuracy of (a) $\hat{\sigma}$ reproduction via the $\hat{\sigma}_{map}$ function (grey bars) and mass flow rate prediction (red bars) and (b) resulting accuracy dispersion of the motive mass flow rate prediction for motive nozzle B.

The statistical analysis of the model accuracy distribution below ±12.5% is presented in Fig. 10 for motive nozzle A (black bars) and motive nozzle B (grey bars). First, the previously described accuracy of the simulation results in the case of the smaller motive nozzle is higher than that of larger motive nozzle

This is the accepted version of an article published in International Journal of Refrigeration
https://doi.org/10.1016/j.ijrefrig.2020.02.015

B. Satisfactory results of very low inaccuracy below ±5.0% were obtained for 70% and 40% of the motive nozzle A and B simulations, respectively. However, almost 80% of the latter is computed with inaccuracy below ±10.0%. Finally, more than 90% of the simulated OC was predicted with inaccuracy below ±12.5%. However, the percentage of highly accurate predictions would be higher if the aforementioned maximum errors would not be included in the analysis presented in Fig. 10.

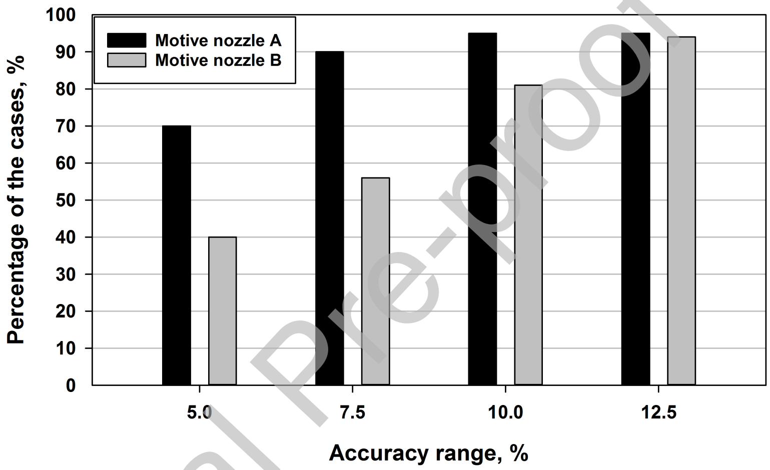

Figure 10: Distribution of the model accuracy in a given range.

The accuracy of the suction stream prediction is presented in Fig. 11a and Fig. 11b for motive nozzles A and B, respectively. The motive nozzle mass flow rate differences for the analysed $k-\epsilon$ and $k-\omega$ turbulence models were negligible, namely below 1.0%. The quality of the suction nozzle mass flow rate prediction is definitely unsatisfactory. In the vast majority of the simulated cases, the inaccuracy of the suction stream prediction was above ±20.0%. Similar to the motive nozzle computations, the accuracy is higher for the larger motive nozzle. However, some proportionality could be indicated in both cases and is especially visible for the smaller motive nozzle. That is, for high motive pressures up to OC #40, the suction stream is overestimated at the level between approx. 20% and 40%. In cases where the pressure is higher than for #40, the motive pressure is below approx. 65 bar, and the suction stream is under-predicted. On the other hand, over 50 cases simulated with the $k-\omega$ turbulence model are characterised by the accuracy higher than 20.0%.

With regard to suction stream and mixing processes, the mathematical model should include physics such as inter-facial slip and cavitation in the pre-mixing chamber. The influence of the turbulence model onto cavitation intensity should be considered as relatively high. Hence, the aforementioned model should be evaluated simultaneously in several aspects due to their mutual interaction. Moreover, the phase change process inside the shock wave pattern in the pre-mixing area should be considered as a more instantaneous than constant evaporation in the motive nozzle. Hence, in this study, the authors focused only on the expansion process in the motive nozzle and the resulting accuracy of the motive stream prediction. In future studies, the aforementioned additional modelling of suction stream behaviour will be considered.

This is the accepted version of an article published in International Journal of Refrigeration
https://doi.org/10.1016/j.ijrefrig.2020.02.015

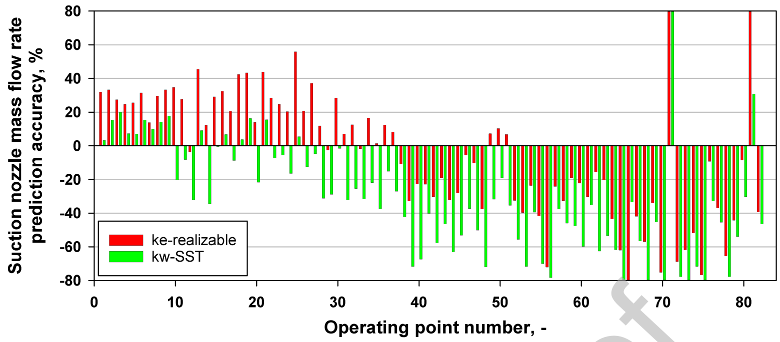

(a) Motive nozzle A

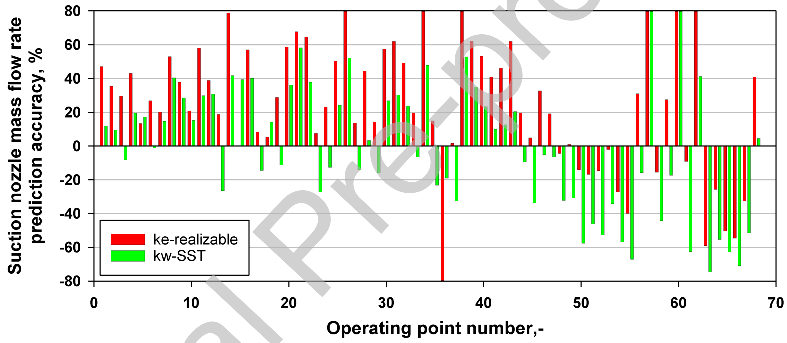

(b) Motive nozzle B

Figure 11: Accuracy of the suction stream prediction for (a) motive nozzle A and (b) motive nozzle B.

6. Results and discussion on the comparison of the HNB and HEM approaches

The developed HNB should be compared to the HEM approach, which was described as the most inaccurate model in the region of low motive pressure, i.e., below 70 bar. For this reason, two representative cases were chosen for further analysis. The first case is OC #4, characterised by high accuracy of the motive mass flow rate prediction equal to -5.0%. The second case considered in this analysis was OC #77, which was much less accurate, i.e. the m_{MN} was underestimated by 38.0%. The flow characteristic was discussed on the basis of the vapour quality profile and fields of absolute pressure and velocity magnitude.

This is the accepted version of an article published in International Journal of Refrigeration
https://doi.org/10.1016/j.ijrefrig.2020.02.015

6.1. Vapour quality profiles

The vapour quality distribution in the area of the ejector motive nozzle is presented in Fig. 12a for OC #4 and Fig. 12b for #77. Moreover, the throat and outlet of the motive nozzle are indicated by vertical dashed and dotted lines, respectively.

As expected, in both cases, the evaporation process of the HEM approach is realised in a dynamic manner. The vast majority of the vapour is generated in the throat region of the motive nozzle where vapour quality is on the level of 0.15-0.25. With regard to the HNB, the vapour generation rate is substantially lower. The first gas bubbles are generated in a slow process, providing less than 0.02 of the vapour mass fraction of the throat. Next, the vapour quality constantly increased along the divergent part of the motive nozzle.

Nevertheless, in the case of OC #4 (Fig. 12a), both approaches reach similar vapour quality, equal to approximately 0.30 at the motive nozzle outlet. However, in the very beginning of the pre-mixing chamber, the HNB predicts significantly higher evaporation than does HEM. According to the motive nozzle outlet, similar vapour quality was obtained in both approaches. Consequently, similarities are visible in the flow fields, such as velocity and pressure. Finally, the mass flow rates at the motive port of the HEM and HNB simulations could be characterised as comparable because they differ by 5.4%.

On the other hand, an analysis of the vapour quality distribution performed for OC #77 (Fig. 12b) revealed some additional differences. In addition to global differences in profile characteristics, the vapour quality for the HNB was significantly lower than that obtained by HEM. That is, the HNB vapour quality and the HEM vapour quality at the motive nozzle outlet were equal to 0.1 and 0.25, respectively. The latter approach could be compared to the OC #4 results where the aforementioned 0.30 level of vapour quality was obtained at the motive nozzle outlet. Hence, the substantial difference in the evaporation process behaviour between OC #4 and #77 is visible only for the HNB. Consequently, simulation of the fluid flow within the HNB approach resulted in the increased accuracy of the m_{MN} prediction (δm = 0.5%) when compared to that obtained for the HEM formulation (δm = -38.0%).

This is the accepted version of an article published in International Journal of Refrigeration
https://doi.org/10.1016/j.ijrefrig.2020.02.015

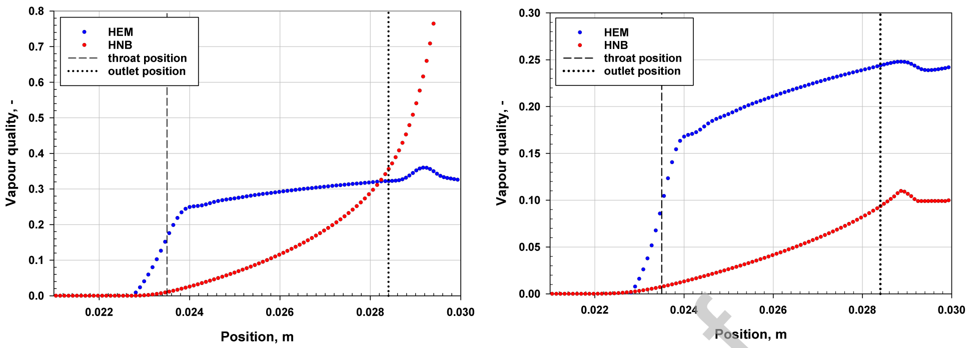

(a) OC #4 (b) OC #77

Figure 12: Vapour quality profiles along the ejector axis for the HEM (blue dots) and HNB (red dots) in the area of motive nozzle and pre-mixing chamber for OC (a) #4 and (b) #77.

6.2. *Velocity and absolute pressure fields*

As discussed above, the crucial difference in the vapour quality profiles of the HEM and those of the HNB were obtained in OC #77. Hence, that case is utilised for further field result analysis. The absolute pressure fields of the motive nozzle area obtained from the HEM and HNB are presented in Fig. 13. Moreover, the corresponding absolute pressure profile is presented along the presented field with the throat and motive nozzle outlet marked by vertical dotted lines. Compared to the HEM formulation, the HNB resulted in a low absolute pressure just before the motive nozzle throat as a consequence of the high motive mass flow rate and resulting intensified pressure drop in the subcritical region. Hence, the absolute pressure in the motive nozzle throat computed by the HNB was lower than that obtained by HEM by approx. 2 bar. In the divergent section, the HEM approach predicted a nearly linear pressure drop from approx. 45 bar (green/yellow colour in Fig. 13) to approx. 27 bar (blue/green in Fig. 13). The HNB computations resulted in smooth pressure reduction at the same distance where almost the entire divergent section corresponds to the green colour, indicating a range between 43 bar and 30 bar. However, the latter approach resulted in a higher intensity of the first pressure drop immediately after the motive nozzle outlet, where approx. 21 bar of minimum absolute pressure was reached. The HEM solution predicted a minimum absolute pressure equal to approx. 25 bar. Finally, a shock wave pattern in the pre-mixing chamber is more visible in the case of the HNB computations where a more uniform pressure distribution was obtained from the HEM simulation.

This is the accepted version of an article published in International Journal of Refrigeration
https://doi.org/10.1016/j.ijrefrig.2020.02.015

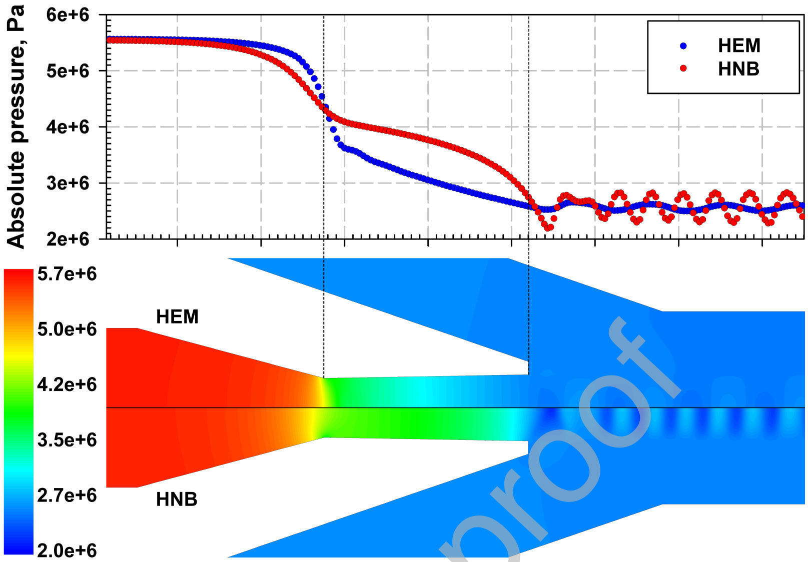

Figure 13: Absolute pressure (Pa) profile and corresponding field distribution for the HEM and HNB approaches for OC #77 in the area of the motive nozzle and pre-mixing chamber.

The field distribution of the velocity magnitude obtained from the HEM and HNB is presented in Fig. 14 with the corresponding profile and lines indicating the throat and motive nozzle outlet. In the convergent part of the motive nozzle, higher velocity was obtained using the HNB as a consequence of the higher motive mass flow rate and constant pressure-specific enthalpy boundary condition. Considering the divergent part, the differences were more significant. Moreover, reflection of the absolute pressure distribution can be found. The HEM results are characterised by a substantial and rapid increase in the velocity, while those of the HNB showed smooth growth of the velocity magnitude along the divergent section of the motive nozzle. Consequently, the HNB delivers approx. 90 $m{\cdot}s^{-1}$ (yellow colour in Fig. 14), and the HEM delivers nearly 120 $m{\cdot}s^{-1}$ (red colour in Fig. 14) at the motive nozzle outlet. The downstream behaviour in the pre-mixing chamber maintains the described differences. Moreover, the velocity in the wall vicinity is significantly higher for HEM as well. In this case, the difference between the models reached almost 10 $m{\cdot}s^{-1}$.

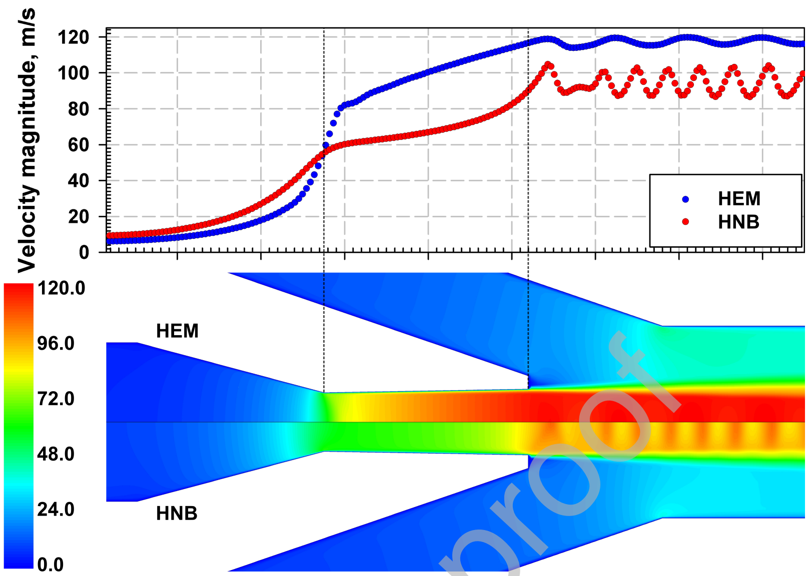

Figure 14: Velocity magnitude (m·s^{-1}) profile and corresponding field distribution for the HEM and HNB for OC #77 in the area of the motive nozzle and pre-mixing chamber.

7. Conclusions

In this study, an expansion model based on the HEM (Smolka et al., 2013) and mixture approaches (Yazdani et al., 2012) was developed to simulate transsonic flow through the R744 ejector. The developed HNB approach was implemented into the *ejectorPL* platform, which allowed for comparison with the previously developed (Smolka et al., 2013) HEM approach. The model structure is suitable for various working fluids (preferable natural refrigerants) after the proper calibration process of the $\widehat{\sigma}$ responsible for the evaporation rate and the resulting motive mass flow rate. In this study, the calibration of the $\widehat{\sigma}$ was performed for a CO_2 two-phase ejector.

- The calibration procedure included various ejector geometries and a wide range of motive nozzle OCs. The calibration range contained motive nozzle pressures from 50 bar to 70 bar, where the HEM model accuracy was unsatisfactory. The criterion of the successful calibration was an accuracy of below 0.5% for the motive mass flow rate prediction.

- The calibrated HNB was validated against experimental data composed of 150 operating points (Tables 3 and 4), which included the mass flow

This is the accepted version of an article published in International Journal of Refrigeration
https://doi.org/10.1016/j.ijrefrig.2020.02.015

rate for validation purposes and pressure and specific enthalpy for the model conditions.

- The validation results were considered as acceptable regarding discrepancy between the experimental and numerical mass flow rates for the whole range of the investigated OC. That is, the discrepancy between the measured and computed mass flow rates was below 10.0% for the vast majority of the cases.

- 70% of the simulated cases were simulated with a mass flow rate prediction below 7.5% of the relative error. The major advantage of the presented model is the high accuracy of the motive mass flow rate predictions. The relative error of the m_{MN} prediction was below 5.0% for over half of the investigated cases.

- The accuracy of the model differs between small and large motive nozzles. Moreover, the fidelity of the presented model was unsatisfactory for only 4 of 150 cases.

- Regarding applicability, the presented methodology introducing the universal two-phase ejector designing tool that could be used for other fluids. An analysis of the vapour quality profiles showed the major difference in evaporation for the HEM simulations and smooth and linear vapour generation in the case of the HNB computations.

- The reason for these differences was found in the absolute pressure and the velocity magnitude fields in the motive nozzle. Consequently, a slower evaporation process resulted in a higher pressure along the motive nozzle in the HNB computations. Simultaneously, the increase in the velocity magnitude was more rapid as a result of the HEM approach.

Further work will be more focused on the mixing process inside the mixer of the device and on the analysis of the suction stream prediction on the basis of the motive nozzle modelling presented in this study. The promising area of investigation should be the slip velocity between the phases, turbulence modelling and cavitation phenomenon in the pre-mixing chamber.

8. Acknowledgements

Scientific work of JB was financed from the budget for science in the years 2017–2021, as a research project 08/060/DG17/0140 under the programme “Diamond Grant". The work of JS was partially financed from a statuary grant 08/060/BK18/0181 funded by Faculty of Energy and Environmental Engineering, Silesian University of Technology, Gliwice, Poland.

References

Anderson, J.D., 1995. Computational fluid dynamics. The basics with applications. McGraw-Hill, New York.

Angielczyk, W., Seynhaeve, J.M., Butrymowicz, D., Bartosiewicz, Y., 2010. 1-D Modelling of Supersonic Carbon Dioxide Two-Phase Flow through Ejector Motive Nozzle, in: International Refrigeration and Air Conditioning Conference at Purdue, Purdue. pp. 1–8.

Ansys, 2019. Fluent 18.2 Documentation.

Banasiak, K., Hafner, A., Kriezi, E.E., Madsen, K.B., Birkelund, M., Fredslund, K., Olsson, R., 2015. Development and performance mapping of a multi-ejector expansion work recovery pack for R744 vapour compression units. International Journal of Refrigeration 57, 265–276.

Besagni, G., 2019. Ejectors on the cutting edge: The past, the present and the perspective. Energy 170, 998–1003.

Bilicki, Z., Kestin, J., Trevor, S., 1990. Physical aspects of the relaxation model in two-phase flow, in: Proceedings of the Royal Society of London.

Bodys, J., Hafner, A., Banasiak, K., Smolka, J., Ladam, Y., 2018. Design and simulations of refrigerated sea water chillers with CO2 ejector pumps for marine applications in hot climates. Energy 161, 90–103.

Carey, V., 2007. Liquid-Vapor Phase-change Phenomena. Taylor and Francis, New York.

Chung, T., 2010. Computational fluid dynamics. 2nd ed., University Press, Cambridge.

Colarossi, M., Trask, N., Schmidt, D.P., Bergander, M.J., 2012. Multidimensional modeling of condensing two-phase ejector flow. International Journal of Refrigeration 35, 290–299.

This is the accepted version of an article published in International Journal of Refrigeration
https://doi.org/10.1016/j.ijrefrig.2020.02.015

Dang Le, Q., Mereu, R., Besagni, G., Dossena, V., Inzoli, F., 2018. Computational Fluid Dynamics Modeling of Flashing Flow in Convergent-Divergent Nozzle. Journal of Fluids Engineering 140.

Downar-Zapolski, P., Bilicki, Z., Bolle, L., Franco, J., 1996. The non-equilibrium relaxation model for one-dimensional flashing liquid flow. International Journal of Multiphase Flow 22, 473–483.

Elbel, S., Hrnjak, P., 2008. Experimental validation of a prototype ejector designed to reduce throttling losses encountered in transcritical R744 system operation. International Journal of Refrigeration 31, 411–422.

Elbel, S., Lawrence, N., 2016. Review of recent developments in advanced ejector technology. International Journal of Refrigeration 62, 1–18.

European Commission, 2014. Regulation (EU) No 517/2014 of the European Parliament and of the Council of 16 April 2014 on fluorinated greenhouse gases and repealing Regulation (EC) No 842/2006 Text with EEA relevance. Official Journal of the European Union 57, 195–230.

European Commission, 2018. EU ratifies Kigali Amendment to the Montreal Protocol | Climate Action.

Giacomelli, F., Mazzelli, F., Milazzo, A., 2016. Evaporation in supersonic CO2 ejectors: analysis of theoretical and numerical models, in: International Conference on Multiphase Flow, Firenze, Italy.

Giacomelli, F., Mazzelli, F., Milazzo, A., 2018. A novel CFD approach for the computation of R744 flashing nozzles in compressible and metastable conditions. Energy 162, 1092–1105.

Haida, M., Banasiak, K., Smolka, J., Hafner, A., Eikevik, T.M., 2016. Experimental analysis of the R744 vapour compression rack equipped with the multi-ejector expansion work recovery module. International Journal of Refrigeration 64, 93–107.

Haida, M., Smolka, J., Hafner, A., Mastrowski, M., Palacz, M., Madsen, K.B., Nowak, A.J., Banasiak, K., 2018a. Numerical investigation of heat transfer in a CO2 two-phase ejector. Energy 163, 682–698.

This is the accepted version of an article published in International Journal of Refrigeration
https://doi.org/10.1016/j.ijrefrig.2020.02.015

Haida, M., Smolka, J., Hafner, A., Ostrowski, Z., Palacz, M., Nowak, A.J., Banasiak, K., 2018b. System model derivation of the CO2 two-phase ejector based on the CFD-based reduced-order model. Energy 144, 941–956.

Haida, M., Smolka, J., Hafner, A., Palacz, M., Banasiak, K., Nowak, A.J., 2018c. Modified homogeneous relaxation model for the R744 trans-critical flow in a two-phase ejector. International Journal of Refrigeration 85, 314–333.

Lemmon, E., Huber, M., McLinden, M., 2010. NIST standard reference database 23: reference fluid thermodynamic and transport properties - REFPROP. 9th ed., National Institute of Standards and Technology, Standard Reference Data Program, Gaithersburg.

Lucas, C., Rusche, H., Schroeder, A., Koehler, J., 2014. Numerical investigation of a two-phase CO2 ejector. International Journal of Refrigeration 43, 154–166.

Mota-Babiloni, A., Navarro-Esbri, J., Barragan-Cervera, A., Moles, F., Peris, B., 2015. Analysis based on EU Regulation No 517 / 2014 of new HFC / HFO mixtures as alternatives of high GWP refrigerants in refrigeration and HVAC systems. International Journal of Refrigeration 52, 21–31.

Nakagawa, M., Berana, M.S., Kishine, A., 2009. Supersonic two-phase flow of CO2 through converging-diverging nozzles for the ejector refrigeration cycle. International Journal of Refrigeration 32, 1195–1202.

Palacz, M., Haida, M., Smolka, J., Nowak, A.J., Banasiak, K., Hafner, A., 2017a. HEM and HRM accuracy comparison for the simulation of CO2 expansion in two-phase ejectors for supermarket refrigeration systems. Applied Thermal Engineering 115, 160–169.

Palacz, M., Smolka, J., Fic, A., Bulinski, Z., Nowak, A.J., Banasiak, K., Hafner, A., 2015. Application range of the HEM approach for CO2 expansion inside two-phase ejectors for supermarket refrigeration systems. International Journal of Refrigeration 59, 251–258.

Palacz, M., Smolka, J., Nowak, A.J., Banasiak, K., Hafner, A., 2017b. Shape optimisation of a two-phase ejector for CO2 refrigeration systems. International Journal of Refrigeration 74, 210–221.

https://doi.org/10.1016/j.ijrefrig.2020.02.015

Purohit, N., Gullo, P., Dasgupta, M.S., 2017. Comparative Assessment of Low-GWP Based Refrigerating Plants Operating in Hot Climates. Energy Procedia 109, 138–145.

Shih, T., Liou, W., Shabbir, A., Yang, Z., Zhu, J., 1995. A New - Eddy-Viscosity Model for High Reynolds Number Turbulent Flows - Model Development and Validation. Computers Fluids 24(3), 227–238.

Singhal, A.K., Athavale, M.M., Li, H., Jiang, Y., 2002. Mathematical Basis and Validation of the Full Cavitation Model. Journal of Fluids Engineering 124, 617.

Smolka, J., Bulinski, Z., Fic, A., Nowak, A.J., Banasiak, K., Hafner, A., 2013. A computational model of a transcritical R744 ejector based on a homogeneous real fluid approach. Applied Mathematical Modelling 37, 1208–1224.

Stadtke, H., 2006. Gasdynamics Aspects of Two-Phase Flow. Wiley-VCH, Weinheim.

United Nations Environment Programme (UNEP), 1987. Montreal Protocol, 1987 .

United Nations Framework Convention on Climate Change (UNFCCC), 1997. Kyoto Protocol, 1997 .

Yazdani, M., Alahyari, A.a., Radcliff, T.D., 2012. Numerical modeling of two-phase supersonic ejectors for work-recovery applications. International Journal of Heat and Mass Transfer 55, 5744–5753.

Yixiang Liao, D.L., 2015. 3d cfd simulation of flashing flows in a converging-diverging nozzle. Nuclear Engineering and Design 292, 149 – 163.

This is the accepted version of an article published in International Journal of Refrigeration
https://doi.org/10.1016/j.ijrefrig.2020.02.015

Nomenclature

HFO	Hydrofluoroolefin	
HNB	Homogeneous non-equilibrium model with boiling phenomenon	
HRM	Homogeneous relaxation model	
HVAC	Heating Ventilation and Air Conditioning	
MER	Mass entrainment ratio	
OC	Operating condition	
Subscripts		
CFD	Computational	
EXP	Experimental	
g	Saturated gas	
l	Saturated liquid	
max	Maximum	
MN	Motive nozzle	
OUT	Outlet	
rec	Amount of the recovered ejector expansion work rate	
sat	Saturation state	
SN	Suction nozzle	
Superscripts		
$\bar{}$	Reynolds-averaged quantities	
$\tilde{}$	Favre-averaged quantities	
Roman Symbols		
c_p	Specific heat	$J{\cdot}kg^{-1}{\cdot}K^{-1}$
D	Diameter	m
E	Total specific enthalpy	$J{\cdot}kg^{-1}$
f	Mass flux	$kg{\cdot}m^{-2}{\cdot}s^{-1}$
G_b	Generation of the turbulence kinetic energy due to buoyancy	$kg{\cdot}m^{-1}{\cdot}s^{-3}$
G_c	Universal gas constant	$J{\cdot}mol^{-1}{\cdot}K^{-1}$
G_k	Generation of the turbulence kinetic energy due to mean velocity gradients	$kg{\cdot}m^{-1}{\cdot}s^{-3}$
h	Specific enthalpy	$J{\cdot}kg^{-1}$
$j_{nw\pm}$	Flux of the molecules	$mol{\cdot}m^{-2}{\cdot}s^{-1}$
k	Turbulent kinetic energy	$m^2{\cdot}s^{-2}$
M	Molecular weight	$g{\cdot}mol^{-1}$
m	Mass flow rate	$kg{\cdot}s^{-1}$
p	Absolute pressure	Pa
R	Vapour generation	$kg{\cdot}m^{-3}{\cdot}s^{-1}$
s	Specific entropy	$J{\cdot}kg^{-1}{\cdot}K^{-1}$
T	Temperature	K
u	Fluid velocity vector	$m{\cdot}s^{-1}$
X	Vapour quality	
Y_M	Contribution of the fluctuating dilatation	$kg{\cdot}m^{-1}{\cdot}s^{-3}$
W	Expansion work rate	W
Greek Symbols		
χ	Mass entrainment ratio	

This is the accepted version of an article published in International Journal of Refrigeration
https://doi.org/10.1016/j.ijrefrig.2020.02.015

δm	Relative error of the mass flow rate	%
ϵ	Turbulent dissipation rate	$m^2 \cdot s^{-3}$
η_{ej}	Ejector efficiency	
Γ	Correction factor to the bulk motion effect	
γ	Angle	°
λ	Thermal conductivity	$W \cdot m^{-1} \cdot K^{-1}$
μ	Dynamic viscosity	$m^2 \cdot s^{-3}$
μ_T	Molecular dynamic viscosity	$m^2 \cdot s^{-3}$
ρ	Fluid density	$kg \cdot m^{-3}$
σ_k	Turbulent Prandtl number for k	
σ_ϵ	Turbulent Prandtl number for ϵ	
τ	Stress tensor	$N \cdot m^{-2}$
$\hat{\sigma}$	Accommodation coefficient	
$\tilde{\sigma}_{map}$	Approximation function	

This is the accepted version of an article published in International Journal of Refrigeration
https://doi.org/10.1016/j.ijrefrig.2020.02.015

Declaration of interests

☒ The authors declare that they have no known competing financial interests or personal relationships that could have appeared to influence the work reported in this paper.

☐The authors declare the following financial interests/personal relationships which may be considered as potential competing interests:

This is the accepted version of an article published in International Journal of Refrigeration
https://doi.org/10.1016/j.ijrefrig.2020.02.015